Regulation of mitochondrial ceramide distribution by members of the BCL-2 family[S]

Tejia Zhang,* Lauren Barclay,[†] Loren D. Walensky,[†,§] and Alan Saghatelian[1,*]

Clayton Foundation Laboratories for Peptide Biology,* Helmsley Center for Genomic Medicine, Salk Institute for Biological Studies, San Diego, CA 92037; Department of Pediatric Oncology,[†] Dana-Farber Cancer Institute and Children's Hospital Boston, and Linde Program in Cancer Chemical Biology,[§] Dana-Farber Cancer Institute, Harvard Medical School, Boston, MA 02215

Abstract **Apoptosis is an intricately regulated cellular process that proceeds through different cell type- and signal-dependent pathways. In the mitochondrial apoptotic program, mitochondrial outer membrane permeabilization by BCL-2 proteins leads to the release of apoptogenic factors, caspase activation, and cell death. In addition to protein components of the mitochondrial apoptotic machinery, an interesting role for lipids and lipid metabolism in BCL-2 family-regulated apoptosis is also emerging. We used a comparative lipidomics approach to uncover alterations in lipid profile in the absence of the proapoptotic proteins BAX and BAK in mouse embryonic fibroblasts (MEFs). We detected over 1,000 ions in these experiments and found changes in an ion with an *m/z* of 534.49. Structural elucidation of this ion through tandem mass spectrometry revealed that this molecule is a ceramide with a 16-carbon N-acyl chain and sphingadiene backbone (d18:2/16:0 ceramide). Targeted LC/MS analysis revealed elevated levels of additional sphingadiene-containing ceramides (d18:2-Cers) in BAX, BAK-double knockout MEFs. Elevated d18:2-Cers are also found in immortalized baby mouse kidney epithelial cells lacking BAX and BAK. These results support the existence of a distinct biochemical pathway for regulating ceramides with different backbone structures and suggest that sphingadiene-containing ceramides may have functions that are distinct from the more common sphingosine-containing species.**—Zhang, T., L. Barclay, L. D. Walensky, and A. Saghatelian. **Regulation of mitochondrial ceramide distribution by members of the BCL-2 family. *J. Lipid Res.* 2015.** 56: **1501–1510.**

Supplementary key words apoptosis • ceramides • lipidomics • mass spectrometry • sphingolipids

The mitochondrial apoptotic pathway follows a highly regulated sequence of events and is dependent on BCL-2 proteins (1). Named after its founding member, the antiapoptotic B-cell lymphoma-2 (2–4), the BCL-2 family includes pro- and antiapoptotic members whose interactions regulate the balance between cell death and survival (1). Oligomerization of the proapoptotic executioner proteins BAX and BAK in the mitochondrial outer membrane leads to mitochondrial outer membrane permeabilization. The permeabilized mitochondria release cytochrome c (cyt c) and additional apoptogenic factors to promote caspase activation and proteolysis (1, 5, 6). Dysregulated expression of BCL-2 proteins is associated with cancer (7) and with autoimmune and neurodegenerative diseases (8, 9).

Murine knockout models of BCL-2 members have proven useful for understanding the cellular functions of these proteins (9, 10). Lymphocytes and fibroblasts from BAX and BAK double-knockout (DKO) mice are resistant to apoptosis induced by a range of death signals, supporting an indispensable role for these proteins in mitochondrial apoptosis (9, 11, 12). Cells from $Bak^{-/-}$ mice could activate both extrinsic and intrinsic apoptotic pathways (11). BAX or BAK is sufficient for anoikis- or serum deprivation-induced cell death (12), implying some degree of functional redundancy between these two proteins.

Although much of apoptosis research has focused on its protein components, evidence supports equally important functions for lipids in promoting or inhibiting apoptosis at the mitochondria (13–17). Execution of the mitochondrial apoptotic program requires mobilization of critical protein factors, such as BCL-2 members and cyt c, which requires structural reorganization within the lipid bilayer (14, 17). The mitochondrial lipid cardiolipin tethers cyt c

This research is supported by an Eli Lilly Fellowship (T.Z.), a Burroughs Wellcome Fund Award (A.S.), a Searle Scholars Award (A.S.), and NIH grant 5R01CA050239 (L.D.W.).

Manuscript received 21 February 2015 and in revised form 6 June 2015.

Published, JLR Papers in Press, June 9, 2015
DOI 10.1194/jlr.M058750

Abbreviations: CE, collision energy; cyt c, cytochrome c; d18:1-Cer, sphingosine-containing ceramide; d18:2-Cer, sphingadiene-containing ceramide; DKO, double-knockout; FA, fatty acid; iBMK, immortalized baby mouse kidney epithelial cell; MEF, mouse embryonic fibroblast; MRM, multiple reaction monitoring; rt, room temperature; SKO, single-knockout; THF, tetrahydrofuran.

[1] To whom correspondence should be addressed.
e-mail: asaghatelian@salk.edu

[S] The online version of this article (available at http://www.jlr.org) contains supplementary data in the form of two tables.

to the inner mitochondrial membrane, and cardiolipin peroxidation during apoptosis is a crucial step in releasing cyt c (18, 19). Previous studies also demonstrate that sphingolipids cooperate with BAX and BAK in promoting membrane permeabilization (20–23). The interplay between lipids and apoptosis led us to speculate that BAX and BAK might regulate mitochondrial lipids.

We reasoned that an LC/MS analysis of the BAX and BAK-regulated lipidome could provide an unbiased view into potential lipid metabolic pathways regulated by BAX and BAK. Our lipidomic analysis of WT and DKO mouse embryonic fibroblasts (MEFs) identified distinct differences in mitochondrial lipid composition between DKO and WT cells, revealing a previously unknown function for BAX and BAK in cellular sphingolipid metabolism.

MATERIALS AND METHODS

Materials

d_{31}-d18:1/16:0 (868516) and d18:1/16:0 (860516) ceramides were from Avanti Polar Lipids; d_{14}-palmitoleic acid (9000431) was from Cayman Chemical; ammonium formate (516961), ammonium hydroxide (338818), and formic acid (06440) were from Sigma-Aldrich; water (BJ365-4), methanol (BJ230-4), isopropanol (BJ323-4), acetonitrile (BJ017-4), chloroform (BJ049-1L), guard column kit (21511-492), and C18 silica (53501-270) were from VWR. C4 silica (214TPB1520) was from Western Analytical Products. C4 and C18 analytical columns with the reported dimensions were from Phenomenex or Dikma Technologies. Chemicals for ceramide synthesis were as follows: Grubbs second-generation catalyst, N-succinimidyl palmitate, palmitoleic acid, triethylamine, and vinyl magnesium bromide (Sigma-Aldrich); (*S*)-*Garner* aldehyde (TCI America); oct-7-enal (Novel Chemical Solutions); heptyltriphenylphosphonium bromide, sodium *bis*(trimethylsilyl)amide, and oxalyl chloride (Alfa Aesar); d18:1 sphingosine (Avanti Polar Lipids); tetrahydrofuran (Acros Organics); and pyridine (Mallinckrodt Chemicals). Additional solvents were from EMD Chemicals.

Tissue culture and harvest

MEFs were maintained at 37°C and 5% CO_2 in DMEM (11965, Life Technologies) with 10% FBS (HyClone or Seradigm), penicillin, streptomycin, nonessential amino acids, and *L*-glutamine (final concentration, 6 mM). Immortalized baby mouse kidney epithelial cells (iBMKs) were maintained in the same medium with 5% FBS, penicillin, streptomycin, and *L*-glutamine (6 mM). All cells were passaged (1:4–1:6) at least three times and harvested at confluency (48–52 h after last passage) by scraping into cold PBS on ice. Cell pellets for lipid extraction were used immediately for extraction or frozen at −80°C until further use. Mitochondria isolation was performed immediately after cell harvesting without freezing.

Mitochondria isolation and lipid extraction

Mitochondria were isolated from MEFs (~2.5×10^8 cells) following a known protocol (24) using a sucrose buffer (250 mM sucrose, 10 mM Tris-HCl, 0.1 mM EGTA·4 Na [pH 7.4]), and isolated mitochondria were used immediately for lipid extraction or stored at −80°C until further use. Lipid extraction was performed with modifications on the Bligh and Dyer procedure (25, 26). Mitochondrial (from ~2.5×10^8 cells) or whole cell (~1.5×10^7 cells) pellets were shaken for 30 s in glass vials (with PTFE-lined caps) with 2 ml:1 ml:1 ml chloroform-methanol-citric acid buffer (100 mM trisodium citrate, 1 M NaCl [pH 3.6]). The vials were vortexed for 15 s and centrifuged at 2,200 *g* at 4°C for 6 min. The organic (bottom) layer containing lipids was carefully taken up with a glass Pasteur pipet, transferred to a new glass vial, and concentrated under nitrogen. Lipids were reconstituted in chloroform and 1/4–1/8 of sample used for LC/MS.

Lipidomic analysis of WT, DKO, and single-knockout MEFs

Lipidomic analysis was performed with an Agilent 1200 Series HPLC online with an Agilent 6220 ESI-TOF (Agilent Technologies). Data were acquired in positive and negative ionization modes. For negative mode, a Gemini (Phenomenex) or Inspire (Dikma Technologies) C18 column (5 µm, 4.6 mm × 50 mm) was used with a guard column (C18, 2 µm frit, 2 mm × 20 mm). Solvent A was 95:5 water-methanol with 0.1% ammonium hydroxide, and solvent B was 60:35:5 isopropanol-methanol-water with 0.1% ammonium hydroxide. For positive mode, a Luna (Phenomenex) C5 or Bio-Bond (Dikma Technologies) C4 column (5 µm, 4.6 mm × 50 mm) was used with a guard column (C4, 2 µm frit, 2 mm × 20 mm). Solvent A was 95:5 water-methanol with 0.1% formic acid and 5 mM ammonium formate, and solvent B was 60:35:5 isopropanol-methanol-water with 0.1% formic acid and 5 mM ammonium formate. Identical gradient was used for both modes. The gradient was held at 0% B between 0 and 5 min, changed to 20% B at 5.1 min, increased linearly from 20% B to 100% B between 5.1 min and 45 min, held at 100% B between 45.1 min and 53 min, and returned to 0% B at 53.1 min and held at 0% B between 53.1 min and 60 min to allow column reequilibration. Flow rate was maintained at 0.1 ml/min between 0 and 5 min to counter the pressure increase caused by chloroform injection. The flow rates were 0.4 ml/min between 5.1 min and 45 min and 0.5 ml/min between 45.1 min and 60 min. Injection volume was 10–30 µl. Capillary, fragmentor, and skimmer voltages were 3.5 kV, 100 V, and 60 V, respectively. Drying gas temperature was 350°C, drying gas flow rate was 10 l/min, and nebulizer pressure was 45 psi. Data were collected in both profile and centroid modes using a mass range of 100–1,500 Da.

Data were analyzed via targeted and untargeted approaches. Targeted analysis of known lipids was performed with manual integration in MassHunter Qualitative Analysis (Agilent Technologies) using a symmetric *m/z* expansion of either 50 or 100 ppm (*m/z* expansions of 20, 50, and 100 ppm were compared and there were no significant differences in peak integration). For untargeted analysis, raw data were converted to .mzXML format using trapper (27) and analyzed by XCMS (28) operated in R with the following parameters: family = "s", plottype = "m", bw = 10, and metlin = 0.15; retention correction (retcor) was iterated at least three times to maximize peak alignment across samples. XCMS output files were filtered by statistical significance ($P \leqslant 0.05$), fold change ($\geqslant 3$), and reproducibility across four independent data sets, and the remaining ions were further verified by manual integration in Qualitative Analysis. Database searches were performed in LIPID MAPS (29) and METLIN (30). A neutral mass of 535.50 was used to search the LIPID MAPS Structural Database (29) using the text/ontology-based search option with a mass expansion of ±0.01 and the METLIN (30) database using the Simple search option with a mass tolerance of ±20 ppm.

For construction of volcano plot (*see* Fig. 2B), ions between 0 and 5 min and 50 and 60 min were removed because these ions fall within the aqueous portions of the LC method and are unlikely to be lipids; the remaining ions between 5 and 50 min were examined in qualitative analysis. Isotopes were manually removed, and the resulting parent ions were graphed by their

XCMS-calculated DKO/WT fold changes (average of three biological replicates) and associated *P* values. Statistical significance was determined by two-tailed Student's *t*-test.

Ceramide quantification, coinjection, and tandem MS

A d_{31}-d18:1/16:0 ceramide standard was used for quantification of endogenous C16-C24 ceramides on the TOF instrument using general profiling conditions. The standard was added to chloroform before lipid extraction to account for metabolite loss during extraction. Tandem MS in positive mode was performed with an Agilent 1200 Series HPLC online with an Agilent 6410 Triple Quad MS (Agilent Technologies) in Product Ion mode. Precursor ions were *m/z* 538.5 (d18:1/16:0 ceramide) and *m/z* 536.5 (d18:2/16:0 and d18:1/16:1 ceramides). Time filter width was 0.07 min. Fragmentor voltage, collision energy (CE), skimmer voltage, and ΔEMV were 132, 26, 15, and 400 V, respectively. Capillary voltage was 4.0 kV, skimmer voltage was 15 V, drying gas temperature was 350°C, drying gas flow rate was 8 l/min, and nebulizer pressure was 35 psi for all Triple Quad measurements. Injection volume was 30 µl.

Tandem MS in negative mode was performed with an Agilent 6500 Series Q-TOF LC/MS system. Precursor ions were *m/z* 534.4892 (d18:2/16:0 and d18:1/16:1 ceramides) and *m/z* 536.5048 (d18:1/16:0 ceramide). Injection volume was 15 µl. VCap, nozzle, skimmer1, and fragmentor voltages were 4,500, 2,000, 0, and 365 V, respectively. CE was 26 V. Octopole RF peak voltage was 750 V. Isolation width was set to Medium. Gas and sheath gas temperatures were 250°C; gas and sheath gas flow rates were 13 l/min and 12 l/min, respectively; and nebulizer pressure was 55 psi. Positive- and negative-mode tandem MS was recorded for mitochondrial and whole cell lipids from WT and DKO MEFs to verify the presence of the same ceramide species in all sample fractions.

The Triple Quad instrument operated in multiple reaction monitoring (MRM) mode was used for coinjection. MEF whole cell lipid extract was used as sample, synthetic Δ4, 11-d18:2/16:0 ceramide was used as standard, and a combination of sample and standard used for coinjection. All samples were dissolved in chloroform such that the final volume was 10 µl. The fragmentor and CE were the same as Product Ion. The transition in negative mode was *m/z* 534.5 → *m/z* 280.3, ΔEMV was 400 V, and MS1 resolution was set to Wide and MS2 resolution to Unit. LC parameters were identical to comparative lipidomics. d_{12}-d18:2/16:0 ceramide was detected by dynamic MRM using the transition *m/z* 548.6 → 274.3 in positive mode. Retention time was 42.55 min, and the retention window was 10 min. All other parameters were identical to coinjection.

Measurement of d18:1/X:0, d18:2/X:0, and d18:1/X:1 ceramides by MRM

Differently saturated ceramide isomers were quantified on the Triple Quad instrument using identical conditions as coinjection. A list of targeted ceramides and associated parameters is provided in supplementary Table 1. Mitochondrial sample (1/4–1/8 from ~2.5×10^8 cells) or 1/3–1/6 of whole cell sample (from ~1.5×10^7 cells) was used for analysis. For each ceramide N-acyl chain, the relative ion abundances of d18:2/X:0 and d18:1/X:0 species were taken as an estimation of the d18:2 to d18:1-Cers ratio.

Syntheses of N-[(2*S*, 3*R*, 4*E*, 11*Z*)-1, 3-dihydroxyoctadeca-4, 11-dien-2-yl]palmitamide (d18:2/16:0 ceramide)

Step 1. Stereoselective addition of vinyl magnesium bromide to (*S*)-*Garner* aldehyde was carried out in tetrahydrofuran (THF), and the crude product was purified by silica gel chromatography based on known procedures (31, 32) to yield (*S*)-*tert*-butyl 4-[(*R*)-1-hydroxyallyl]-2,2-dimethyloxazolidine-3-carboxylate (**1**) for synthesis of d18:2/16:0 ceramide (**Fig. 1A**, **1**).

Step 2. (S)-tert-BUTYL 4-[(R, E)-1-HYDROXY-9-OXONON-2-EN-1-YL]-2, 2-DIMETHYLOXAZOLIDINE-3-CARBOXYLATE. To a solution of **1** (280 mg, 1.1 mmol, 1 eq.) in dry dichloromethane (10 ml) were added oct-7-enal (549 mg, 660 µl, 4.4 mmol, 4 eq.) and Grubbs second-generation catalyst (23 mg, 0.027 mmol, 0.025 eq.). The solution was refluxed overnight (~16 h), and completion of reaction was confirmed by TLC (40:60 ethyl acetate-hexanes, PMA stain, R_f = 0.35–0.4). The reaction was concentrated and purified by silica gel chromatography (35:65 ethyl acetate-hexanes). Fractions containing product were concentrated to afford **2** (190 mg, 49% yield) as a colorless oil. ^{1}H-NMR (500 MHz, $CDCl_3$): 1.19–1.54 (*m*, 21H), 1.94 (*dt*, 2H), 2.31 (*t*, 2H), 3.73–4.07 (*m*, 5H including OH), 5.35 (*dd*, J = 15.3, 6.3, 1H), 5.9 (*m*, 1H), 9.64 (*s*, 1H). ESI-MS: theoretical *m/z* for $C_{19}H_{33}NO_5Na^+$ (sodium adduct): 378.2251, detected *m/z*: 378.2224, ppm difference: 7.14 (Fig. 1A, **2**).

Step 3. (S)-tert-BUTYL 4-[(R, 2E, 9Z]-1-HYDROXYHEXADECA-2, 9-DIEN-1-YL)-2, 2-DIMETHYLOXAZOLIDINE-3-CARBOXYLATE. To a suspension of heptyltriphenylphosphonium bromide (330 mg, 0.75 mmol, 3 eq.) in dry THF (10 ml) at 0°C was added sodium *bis*(trimethylsilyl)amide (725 µl of 1 M solution in dry THF, 2.9 mmol, 2.9 eq.). The solution immediately turned orange and was stirred at 0°C for 30 min. The resulting solution was cooled to −78°C, and a THF solution (2 ml) of **2** (90 mg, 0.25 mmol, 1 eq.)

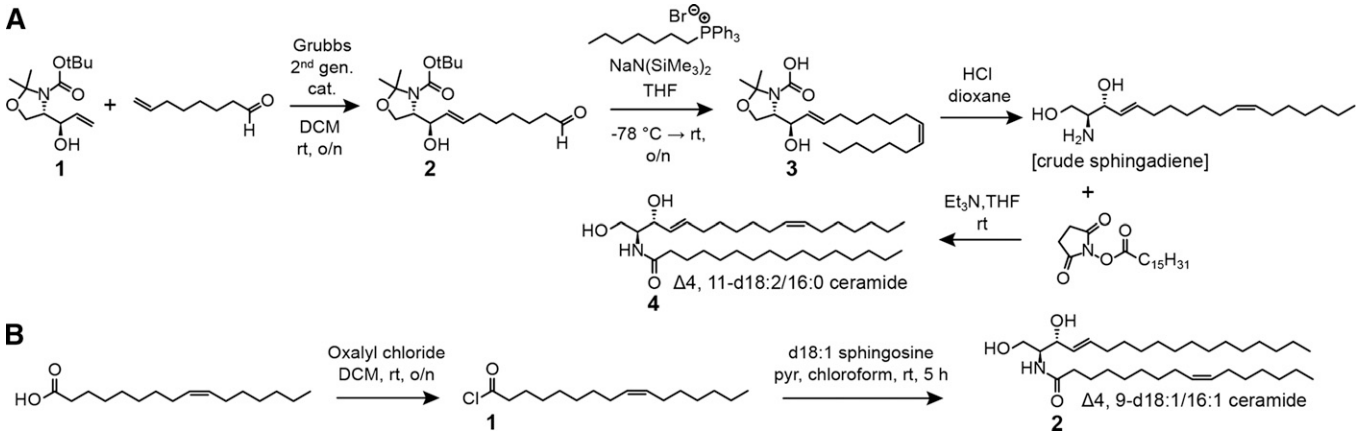

Fig. 1. Chemical synthesis. A: Synthesis of d18:2/16:0 ceramide. B: Synthesis of d18:1/16:1 ceramide.

was added. The reaction was allowed to proceed overnight where it warmed from −78°C to room temperature (rt) and the color dissipated until white. Saturated aqueous sodium bicarbonate was added, and the aqueous phase was extracted three times with diethyl ether (10 ml). The combined organic phases were washed with brine, dried over anhydrous sodium sulfate, concentrated, and purified by silica gel chromatography (15:85 ethyl acetate-hexanes, $R_f = 0.3$) to yield **3** (36 mg, 32% yield) as a colorless oil. ^{1}H-NMR (400 MHz, $CDCl_3$): 0.88 (*t*, 3H), 1.25–1.62 (*m*, 29H), 2.02 (*m*, 6H), 3.83 (*m*, 1H), 4.02 (*m*, 1H), 4.14 (*m*, 2H), 5.34 (m, 2H), 5.44 (*dd*, J = 15.3, 5.2, 1H), 5.73 (*m*, 1H). ESI-MS: theoretical *m/z* for $C_{26}H_{47}NO_4Na^+$ (sodium adduct): 460.3397, detected *m/z*: 460.3388, ppm difference: 1.96 (Fig. 1A, **3**).

Step 4. N-([2S, 3R, 4E, 11Z]-1, 3-dihydroxyoctadeca-4, 11-dien-2-yl)palmitamide. A solution of **3** (33 mg, 0.076 mmol, 1 eq.) in 1 M HCl (0.75 ml) and dioxane (0.75 ml) was heated at 100°C for 1 h. The mixture was cooled to rt, neutralized with 1 M NaOH (1 ml), and extracted twice with ethyl acetate (3 ml). The combined organic phases were sent through a plug of sodium sulfate and concentrated to yield crude sphingadiene. The yellowish solid was dissolved in THF (0.5 ml), and N-succinimidyl palmitate (40 mg, 0.11 mmol, 1.5 eq.) was added, followed by triethylamine (22 µl). After stirring overnight, 1 M HCl (1 ml) was added and the mixture extracted twice with ethyl acetate (2 ml). The combined organic phases were dried over anhydrous sodium sulfate, concentrated, and purified by silica gel chromatography (66:34 ethyl acetate-hexanes, $R_f = 0.5$) to yield **4** (17 mg, 41% yield) as a white solid. ^{1}H-NMR (500 MHz, $CDCl_3$): 0.88 (*m*, 6H), 1.25–1.35 (*m*, 46H), 1.63 (*m*, 2H), 2.00–2.08 (*m*, 6H), 2.25 (*t*, J = 7.5, 2H), 2.88 (s, 1H), 3.70 (m, 1H), 3.88–3.96 (m, 2H), 4.3 (*m*, 1H), 5.34 (m, 1H), 5.53 (*dd*, J = 15.5, 6.5, 1H), 5.78 (*m*, 1H), 6.29 (d, J = 7.5, 1H). ESI-MS: theoretical *m/z* for $C_{34}H_{66}NO_3^+$ (hydrogen adduct): 536.5037, detected *m/z*: 536.5029; ppm difference: 1.49 (Fig. 1A, **4**).

Synthesis of (*Z*)-N-([2*S*, 3*R*, *E*]-1, 3-dihydroxyoctadec-4-en-2-yl)hexadec-9-enamide (d18:1/16:1 ceramide)

To a stirring solution of (*Z*)-hexadec-9-enoic acid (palmitoleic acid, 9.7 mg, 0.041 mmol, 1 eq.) at rt was added oxalyl dichloride (1 ml, excess). Bubble formation was observed over the next 30 min, and the reaction was stirred overnight at rt before being concentrated to afford the crude (*Z*)-hexadec-9-enoyl chloride (**1**). Compound 1 was dried under vacuum for 3 h, dissolved in a mixture of pyridine (15.1 µl, 0.195 mmol, 4.8 eq. assuming 100% yield for previous reaction) and chloroform (0.5 ml) and added dropwise to a stirring solution of (2*S*, 3*R*, *E*)-2-aminooctadec-4-ene-1,3-diol (d18:1 sphingosine, 14.7 mg, 0.049 mmol, 1.2 eq. assuming 100% yield for previous reaction) in chloroform (4 ml). The reaction was stirred at rt for 5 h, water was added, and the resulting mixture was extracted three times with chloroform. The combined organic layers were washed with brine, dried with sodium sulfate, filtered, and concentrated to afford the crude (*Z*)-N-([2*S*, 3*R*, *E*]-1, 3-dihydroxyoctadec-4-en-2-yl)hexadec-9-enamide (**2**), which was used directly for tandem MS. ESI-MS: theoretical *m/z* for $C_{34}H_{64}NO_3^-$ (loss of hydrogen): 534.4892; detected *m/z*: 534.4903; ppm difference: 2.06.

Cellular production of d_{12}-d18:2/16:0 ceramide

For each sample, 20 µl 83 mM d_{14}-palmitoleic acid in DMSO was mixed with 10.5 ml MEF media, and 10 ml of the media introduced to DKO MEFs in a 10 cm tissue culture dish. 20 µl DMSO was used as negative control. Treated cells were incubated at 37°C for 2 h or 21 h before harvest by scraping into cold PBS on ice and lipid extraction.

RESULTS

Comparative metabolite profiling reveals elevated levels of unsaturated C16 ceramide in DKO mitochondria

Lipids were extracted (25, 26) from WT and DKO MEF mitochondria (24) and subjected to LC/MS to identify lipidomic changes in the absence of BAX and BAK (**Fig. 2A**). Major lipid classes (free fatty acids, phospholipids, sphingolipids, acylglycerols, acylcarnitines, ether lipids,

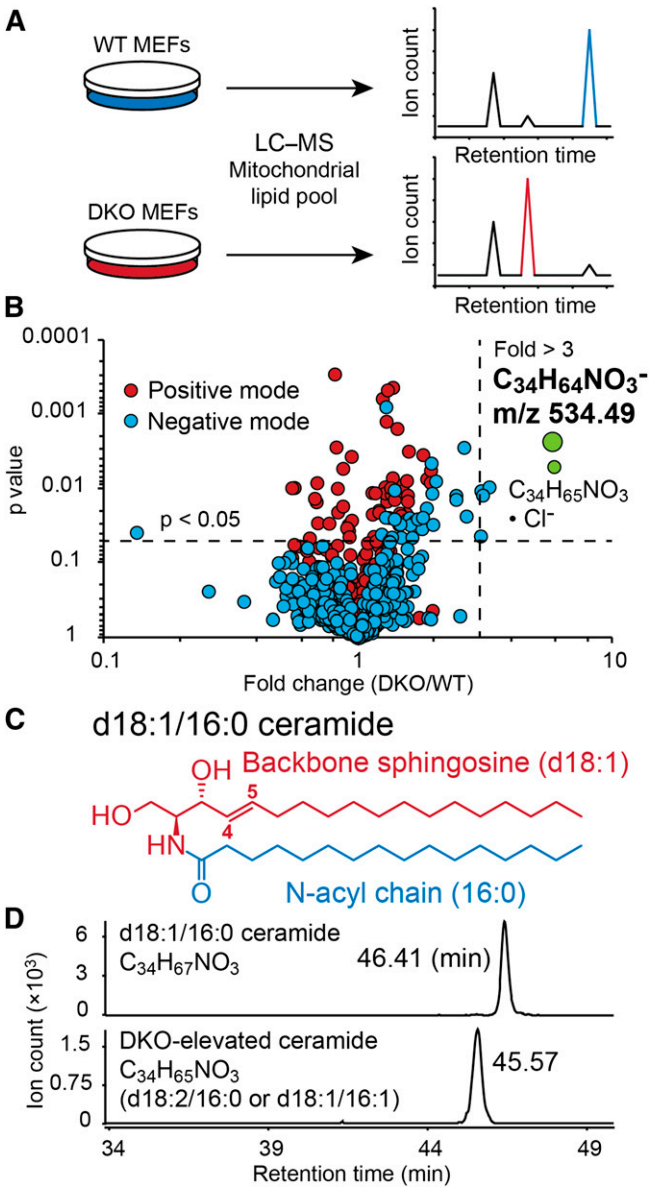

Fig. 2. Comparative lipidomics reveals selective upregulation of diunsaturated ceramides in DKO MEF mitochondria. A: Schematic of comparative lipidomics enabling identification of lipid changes between WT and DKO samples. B: Volcano plot of detected parent ions plotted as DKO/WT fold change versus *P* value (n = 3); the DKO-elevated *m/z* 534 metabolite and its chlorine adduct are in green. C: Structure of d18:1/16:0 ceramide. The *trans* double bond is found at C4-C5 of the sphingosine backbone. D: DKO-elevated ceramide elutes ~1 min before d18:1/16:0 ceramide, in agreement with the commonly observed phenomenon of decreasing retention time with increasing unsaturation in reversed-phase chromatography (37).

cardiolipins, cholesterol, and cholesterol esters) from four independent data sets were analyzed to ensure data quality and reproducibility. Levels of most lipids were unaltered between WT and DKO MEFs (supplementary Table 2), demonstrating that the majority of lipid pathways were unaffected by the absence of BAX and BAK.

Data analysis was also performed using the XCMS software package (28), which aligns, quantifies, and statistically ranks changes in detected ions between WT and DKO groups. XCMS uncovered a metabolite with a detected *m/z* of 534.4886 in negative ionization mode that was consistently elevated in DKO mitochondria relative to WT (Fig. 2B). Our finding indicates that the loss of BAX and BAK can influence cellular metabolism, and the observation of one change in a background of mostly unaltered metabolites demonstrates specificity in the metabolic pathway regulated by BAX and BAK.

A database search [LIPIDMAPS (29) and METLIN (30)] with the exact neutral mass of the DKO-elevated metabolite afforded the molecular formula $C_{34}H_{65}NO_3$, corresponding to the sphingolipid ceramide. Mammalian ceramides are typically comprised of a sphingosine, with a *trans* double bond at C4-C5 (Fig. 2C, red) and an N-acyl fatty acid (Fig. 2C, blue) (33–35). One of the major mammalian ceramides is d18:1/16:0 (Fig. 2C), which has the molecular formula $C_{34}H_{67}NO_3$ (33, 36). The DKO-elevated ceramide ($C_{34}H_{65}NO_3$) contains two fewer hydrogens, or one more double bond, than the d18:1/16:0 species. This is consistent with the earlier observed LC retention time for the DKO-elevated ceramide (Fig. 2D) (37). The structure of the DKO-elevated ceramide is, therefore, d18:2/16:0 or d18:1/16:1, and the second double bond is present in either the backbone (i.e., sphingadiene-containing ceramide) or the N-acyl chain. We refer to ceramides with two double bonds as "diunsaturated ceramides" and ceramides with one double bond as "monounsaturated ceramides."

Diunsaturated ceramides are upregulated in DKO MEF mitochondria

To account for less abundant diunsaturated ceramides not identified during untargeted XCMS analysis, monounsaturated and diunsaturated C16–C24 ceramide levels were measured by isotope-dilution MS (26, 38). A d_{31}-d18:1/16:0 ceramide standard was added to biological samples during lipid extraction, allowing ratiometric quantification of endogenous ceramides. For each N-acyl chain, both the monounsaturated and diunsaturated species were considered.

Of all detectable ceramides (**Fig. 3A**), ceramides with C16 acyl chains occurred at the highest level (~300–1,400 pmol/mg protein). The next highest level belonged to ceramides, with C24 acyl chains (~150–600 pmol/mg protein) (Fig. 3B). A decrease in cellular concentration was observed for C18 and C20 ceramides (Fig. 3B), corresponding to an ~100-fold decrease relative to C16 ceramides (Fig. 3B). Comparison of WT and DKO MEFs revealed a unique change in the ceramide profile. Levels of most monounsaturated ceramides (i.e., d18:1/16:0) were unaltered between WT and DKO MEF mitochondria. By contrast, a significant increase (~2–4.5-fold) in most diunsaturated ceramides was observed in the absence of BAX and BAK (Fig. 3B). This increase led to an ~2-fold rise in the total diunsaturated-to-monounsaturated mitochondrial ceramide ratio (Fig. 3C, D).

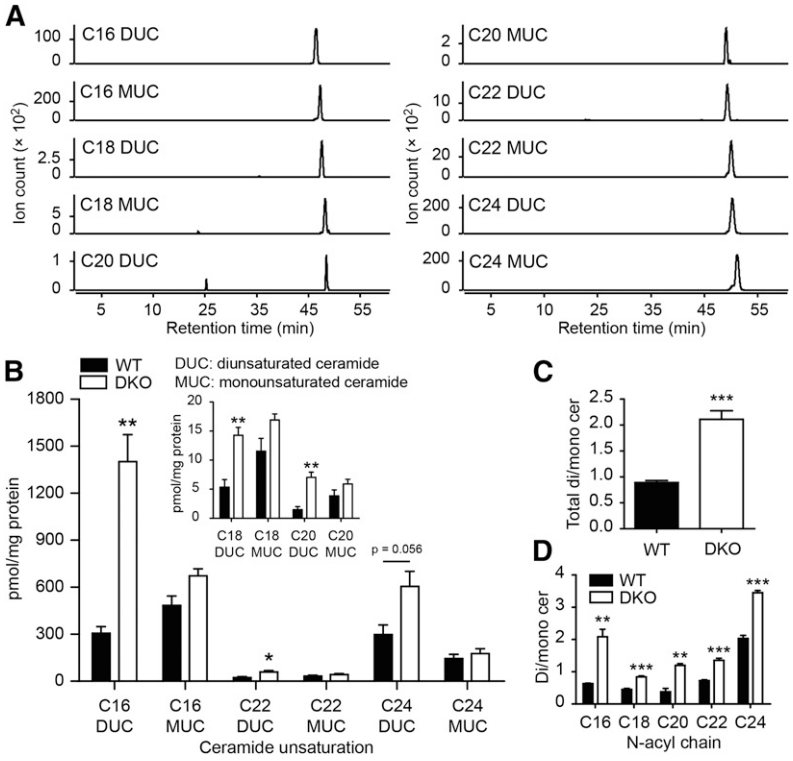

Fig. 3. Selective elevation of diunsaturated ceramides requires BAX and BAK. A: Extracted ion chromatograms of C16-C24 ceramides. *m/z* expansion: ±50 ppm. B: Quantification of C16-C24 ceramides with d_{31}-d18:1/16:0 ceramide as internal standard. C: Total mitochondrial di/monounsaturated ceramide ratios for WT and DKO MEFs. D: WT and DKO MEF mitochondrial di/monounsaturated ceramide ratio by N-acyl chain. * $P \leq 0.05$, ** $P \leq 0.01$, and *** $P \leq 0.001$, two-tailed Student's *t*-test (SEM; n = 3 for all sections).

We also monitored the levels of additional sphingolipids. No differences in additional sphingolipids or in palmitic or palmitoleic acids were observed between WT and DKO MEF mitochondria (**Fig. 4A**, B; supplementary Table 2), indicating that changes in ceramides are not the direct consequence of an alteration in the fatty acid composition or in other sphingolipids. Most ceramides were also unchanged between WT and BAX or BAK single-knockout (SKO) MEFs (Fig. 4C, D), suggesting that elevation of these diunsaturated ceramides required both BAX and BAK.

DKO-elevated metabolite is d18:2/16:0 ceramide

To locate the double bonds in the DKO-regulated diunsaturated ceramide, we compared the fragmentation profile of d18:1/16:0 ceramide with the diunsaturated C16 ceramide. Positive-mode tandem MS of d18:1/16:0 ceramide yielded the sphingoid backbone-derived product ions *m/z* 282, 264, and 252 (**Fig. 5A**) (39–41). Tandem MS of the DKO-regulated diunsaturated C16 ceramide yielded the product ions *m/z* 280, 262, and 250; each of these ions is 2 Da lower in mass than the corresponding product ion from the d18:1/16:0 ceramide (Fig. 5A). Thus, the structure of the DKO-elevated diunsaturated C16 ceramide is d18:2/16:0. Negative-mode tandem MS was also consistent with this structural assignment, as the 2-Da mass shift was observed only for product ions from the sphingoid backbone (Fig. 5B).

Identical fragmentation patterns were observed between the DKO-elevated ceramide and the synthetic d18:2/16:0 ceramide standard (Fig. 5C). For the initial synthesis, we installed the *cis* double bond in the d18:2/16:0 ceramide at C11-C12 (Fig. 1A). A double bond at this position would arise from potential incorporation of palmitoleyl (Δ9-*cis*-16:1)-CoA during de novo ceramide biosynthesis (34, 42) (also see DISCUSSION). In a coelution study, this synthetic Δ4, 11-d18:2/16:0 ceramide standard overlapped with the DKO-elevated ceramide (Fig. 5D). Thus, Δ4, 11-d18:2/16:0 ceramide could be contributing toward the BAX, BAK-regulated d18:2 ceramide pool in cells. However, we cannot rule out the presence of multiple d18:2/16:0 ceramide double-bond isomers (35, 43–45) coeluting with this peak. We designate sphingadiene-containing diunsaturated ceramides as d18:2-Cers.

BAX and BAK regulate d18:2-Cers in two different cell types

We next used a targeted MRM detection method to measure all detectable d18:2- and d18:1-ceramides (supplementary Table 1) in MEF and iBMKs. The absence of BAX and BAK raised the levels of C16-C24 d18:2-Cers relative to monounsaturated ceramides in both cell lines (**Fig. 6A**, B). Thus, BAX and BAK regulate d18:2-Cers in at least two distinct cell lines. BCL-2 regulation of these ceramides is also highly specific; d18:2-Cers were upregulated, whereas other diunsaturated ceramides (e.g., d18:1/16:1) were unchanged (Fig. 6C). Therefore, the location of the additional double bond in the backbone sphingosine is essential for ceramide regulation by BAX and BAK.

DISCUSSION

Several BCL-2 proteins affect cellular metabolism, including glucose and fatty acid metabolism (46–48), calcium homeostasis (49), and insulin secretion (50). Similar to these findings, our data demonstrate a novel metabolic function for BAX and BAK in the regulation of endogenous ceramides. Specifically, we find that BAX and BAK preferentially regulate diunsaturated, sphingadiene-containing ceramides (d18:2-Cers). The presence of the second double bond in the sphingoid

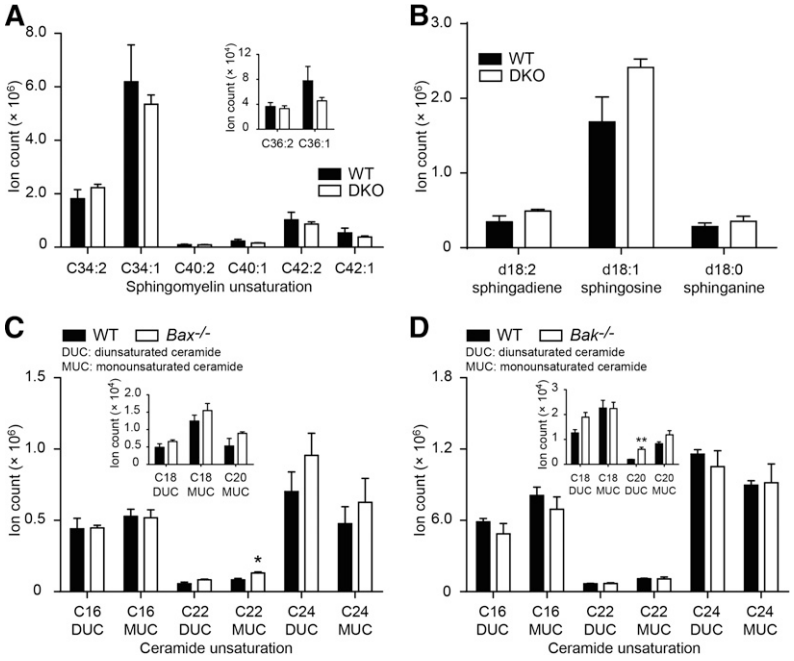

Fig. 4. Additional sphingolipids and ceramide levels in WT, DKO, and SKO MEFs. A: Relative sphingomyelin levels in WT and DKO MEF mitochondria. No statistically significant changes were observed. B: Relative sphingadiene, sphingosine, and sphinganine levels in WT and DKO MEF mitochondria. No statistically significant changes were observed. C: Relative C16-C24 ceramide levels in WT and $Bax^{-/-}$ MEF mitochondria. D: Relative C16-C24 ceramide levels in WT and $Bak^{-/-}$ MEF mitochondria. * $P \leq 0.05$ and ** $P \leq 0.01$, two-tailed Student's *t*-test (SEM; n = 3 for C and D).

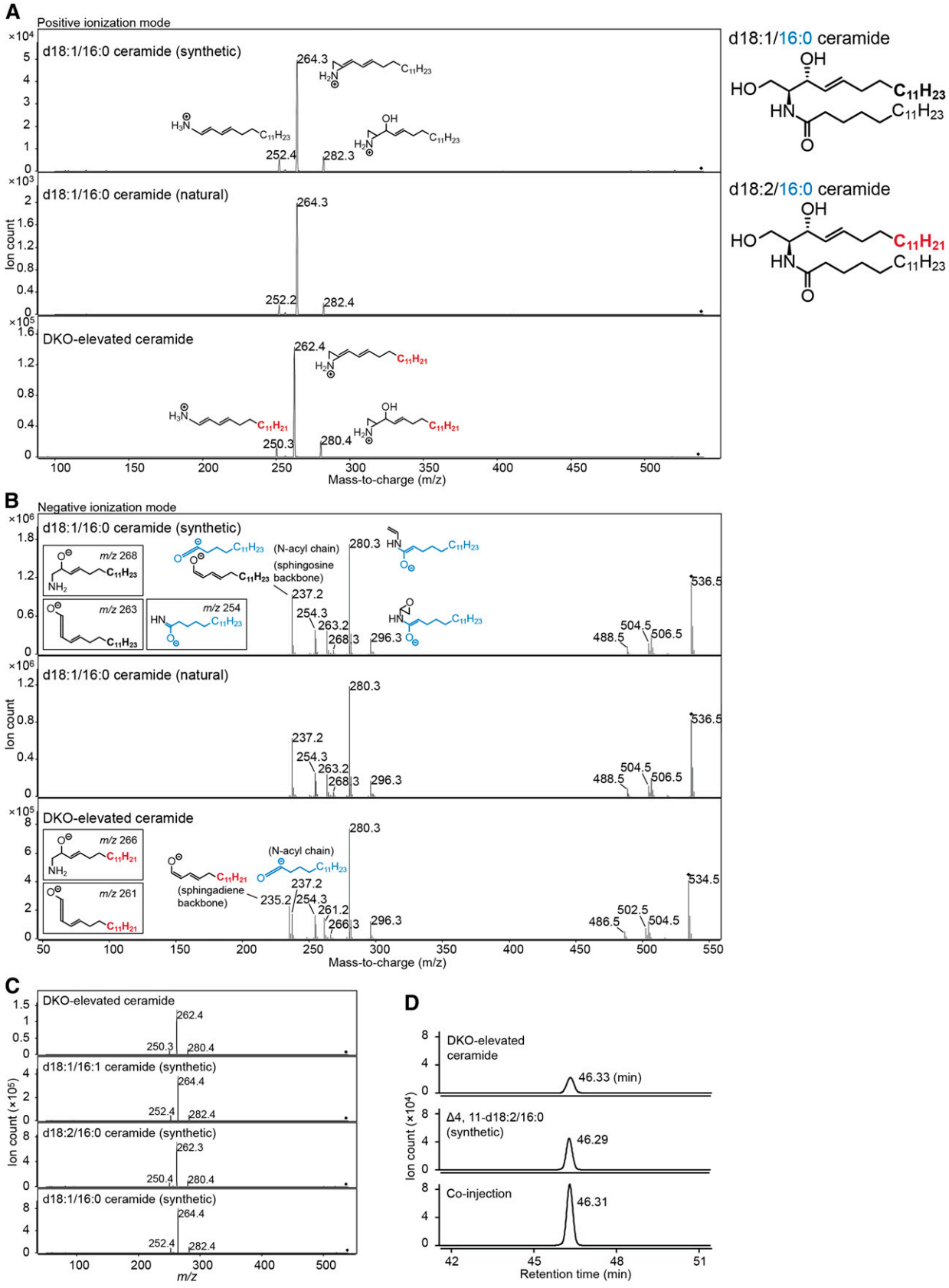

Fig. 5. Structural identification of C16 diunsaturated ceramide. A: Positive ionization mode tandem MS of synthetic and endogenous d18:1/16:0 ceramide and the DKO-elevated ceramide. B: Negative-mode tandem MS of synthetic and endogenous d18:1/16:0 ceramide and the DKO-elevated ceramide. N-acyl chain-derived fragments are in blue. C: Tandem MS of the DKO-elevated ceramide, and synthetic d18:1/16:1, d18:2/d16:0 and d18:1/16:0 ceramides in positive ionization mode. D: Coinjection with synthetic and natural d18:2/16:0 ceramides. All illustrated fragmentations are based on published predictions (39, 41, 59–63).

JOURNAL OF LIPID RESEARCH

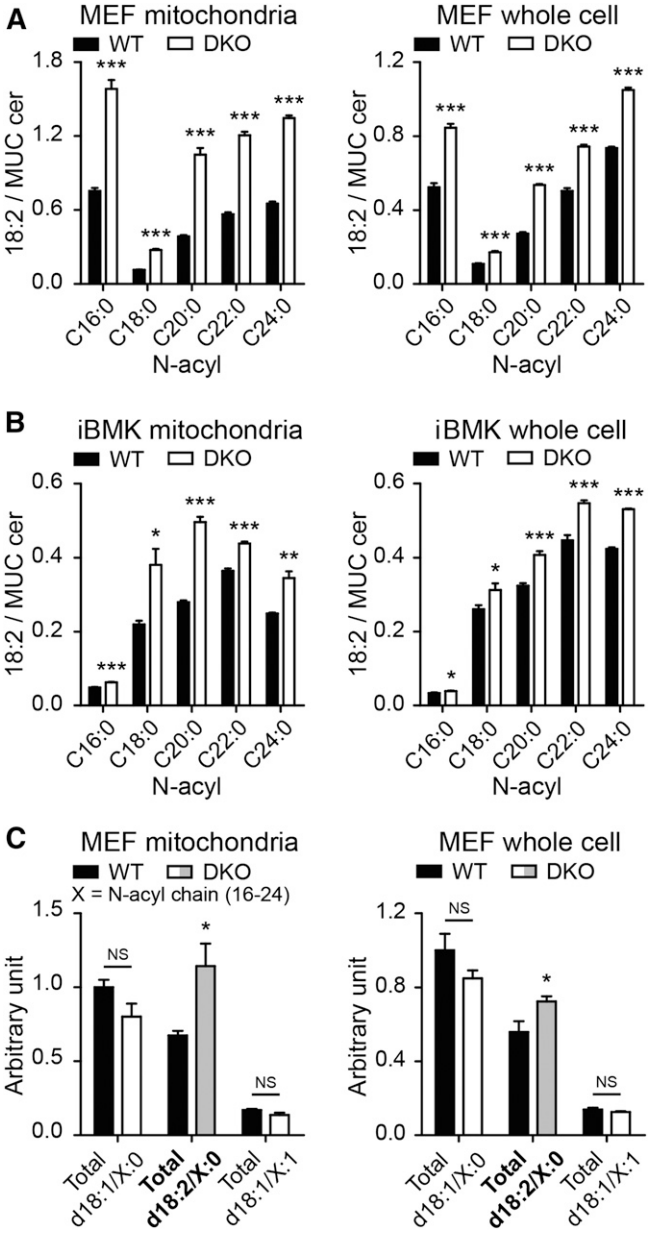

Fig. 6. BAX and BAK selectively regulate d18:2-Cers in MEFs and iBMKs. A: WT and DKO MEF mitochondrial and whole cell d18:2-Cer/d18:1-Cer ratio by N-acyl chain. B: WT and DKO iBMK mitochondrial and whole cell d18:2-Cer/d18:1-Cer ratio by N-acyl chain. C: Total d18:1/X:0, d18:2/X:0, and d18:1/X:1 ceramide levels in WT and DKO MEFs; data are normalized to WT d18:1/X:0 value. * $P \leqslant 0.05$, ** $P \leqslant 0.01$, and *** $P \leqslant 0.001$, two-tailed Student's *t*-test (SEM; n = 4 for all sections).

backbone (i.e., d18:2-Cers) is essential for BAX and BAK regulation. Diunsaturated ceramides with the second double bond in the N-acyl chain were not regulated by BAX and BAK. Ceramide levels were also unaltered in BAX or BAK SKO MEFs, suggesting that BAX and BAK compensate for each other in this metabolic function. Whereas mitochondrial morphogenesis depends on both BAX and BAK (51), only BAK is required for long-chain d18:1-Cers release in response to a range of apoptotic agents (21, 22). Our observation that d18:2-Cers, but not d18:1-Cers, are regulated by both BAX and BAK supports the existence of subpopulations of structurally distinct ceramides that could be selectively modulated by different BCL-2 proteins. To our knowledge, this is the first example of ceramide regulation based on backbone structure, and this result suggests that the backbone specificity in ceramide biosynthetic enzymes requires exploration.

This metabolic function of BAX and BAK is likely connected to their apoptotic function because of the proapoptotic activity of ceramides (15). Ceramides are bioactive lipids involved in multiple cellular processes, including apoptosis, proliferation, and autophagy (17). Cellular ceramide levels rise in response to a range of apoptotic signals (22), and ceramide macrodomains in the outer mitochondrial membrane act as sites of BAX activation during irradiation-induced apoptosis (52). Although numerous studies have demonstrated a proapoptotic role for ceramides, the apoptotic functions of ceramides also depend on lipid structure. Dihydroceramide inhibits ceramide channel formation in isolated mitochondria (53), and long-chain and very long-chain ceramides have been shown to exhibit opposite effects toward cancer cell survival (54). Our discovery of preferential regulation of d18:2-Cers by BAX and BAK suggests that there could also exist distinct cellular ceramide pools with different influences over cellular viability, which we will investigate in future studies.

Sphingadiene-containing sphingolipids are not new. Sphingadienes with a *trans* double bond at C4 and a *cis* double bond at C14 are a component of human serum sphingomyelins (43, 44). Sphingadienes with 14 or 16 carbons and conjugated *cis* double bonds at C4, 6 are present in *Drosophila* (55), and *cis*-C4, 8-sphingadienes are found in plants (56). C16 sphingoid backbones are also present in human plasma due to the activity of an additional serine palmitoyltransferase isoform (SPTLC3) that favors myristoyl (C14:0)-CoA (35, 45). Although there could be multiple biochemical pathways or dietary sources for generating mammalian sphingadiene-containing ceramides (**Fig. 7A**), we have examined the incorporation of unsaturated palmitoleic acid (d_{14}-C16:1 fatty acid [FA]) into the sphingoid backbone. d_{14}-16:1 FA-treated cells produced labeled ceramides to suggest that unsaturated FA incorporation could be one of the routes toward d18:2-Cers production (Fig. 7B). Additional questions, such as the known preference of serine palmitoyltransferases for palmitoyl-CoA over *cis*-unsaturated fatty acyl-CoA substrates (57, 58) and how differently saturated cellular FA pools could be directed toward biosynthesis of sphingosine- or sphingadiene-containing ceramides, will need to be further addressed.

The discovery of the DKO-elevated d18:2-Cers relied on tandem MS. Most research into the role of ceramides in apoptosis focuses on the levels and functions of d18:1-Cers (15). Our work indicates that it would be of interest to revisit these studies using tandem MS and targeted LC/MS approaches to evaluate whether d18:2-Cers were overlooked.

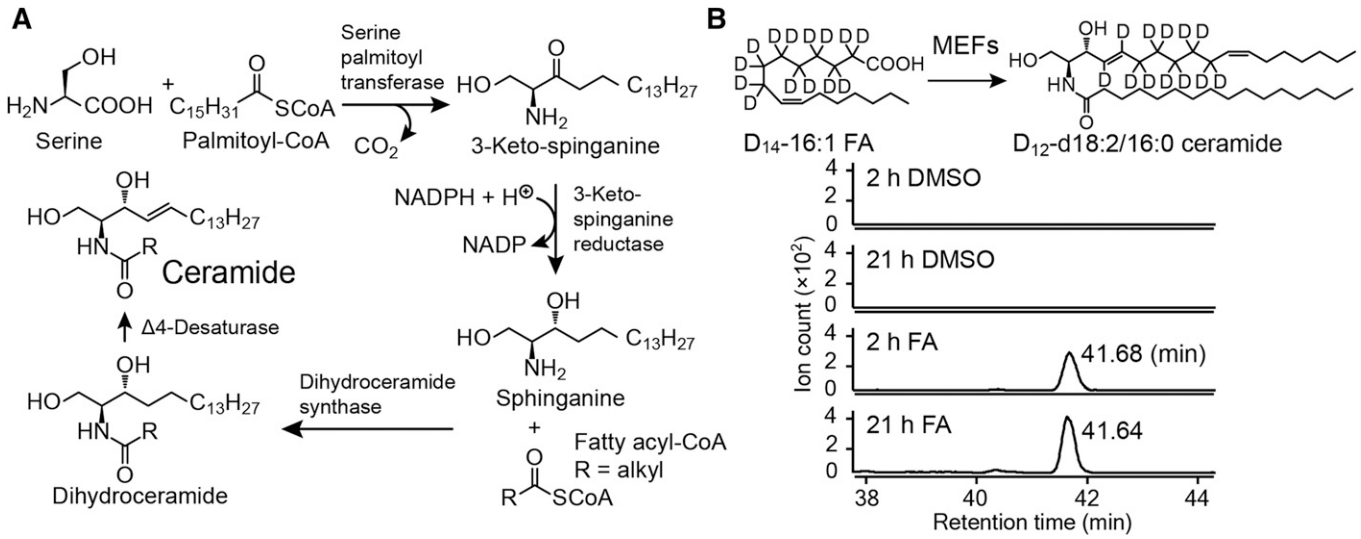

Fig. 7. De novo biosynthesis of d18:2/16:0 ceramide via incorporation of unsaturated fatty acid precursor. A: De novo ceramide biosynthetic pathway condenses a free fatty acyl-CoA with serine to produce the unique sphingosine backbone (34). B: Generation of d_{12}-d18:2/16:0 ceramide by d_{14}-palmitoleic acid-treated MEFs.

The authors thank Prof. Eileen White for the generous gift of WT and DKO iBMK cells; Dr. Sunia A. Trauger at the Harvard FAS Small Molecule Mass Spectrometry core for acquisition of the negative mode ceramide tandem MS spectra; Dr. Qian Chu and Dr. Christopher Vickers for manuscript reviews; and members of the Saghatelian and Walensky research groups for general technical guidance and discussions.

REFERENCES

1. Walensky, L. D. 2006. Bcl-2 in the crosshairs: Tipping the balance of life and death. *Cell Death Differ.* **13:** 1339–1350.
2. Tsujimoto, Y., J. Gorham, J. Cossman, E. Jaffe, and C. Croce. 1985. The t(14;18) chromosome translocations involved in b-cell neoplasms result from mistakes in vdj joining. *Science.* **229:** 1390–1393.
3. Bakhshi, A., J. P. Jensen, P. Goldman, J. J. Wright, O. W. McBride, A. L. Epstein, and S. J. Korsmeyer. 1985. Cloning the chromosomal breakpoint of t(14;18) human lymphomas: Clustering around jh on chromosome 14 and near a transcriptional unit on 18. *Cell.* **41:** 899–906.
4. Cleary, M. L., and J. Sklar. 1985. Nucleotide sequence of a t(14;18) chromosomal breakpoint in follicular lymphoma and demonstration of a breakpoint-cluster region near a transcriptionally active locus on chromosome 18. *Proc. Natl. Acad. Sci. USA.* **82:** 7439–7443.
5. Fletcher, J. I., and D. C. S. Huang. 2006. Bh3-only proteins: Orchestrating cell death. *Cell Death Differ.* **13:** 1268–1271.
6. Gavathiotis, E., M. Suzuki, M. L. Davis, K. Pitter, G. H. Bird, S. G. Katz, H-C. Tu, H. Kim, E. H. Y. Cheng, N. Tjandra, et al. 2008. Bax activation is initiated at a novel interaction site. *Nature.* **455:** 1076–1081.
7. Yip, K. W., and J. C. Reed. 2008. Bcl-2 family proteins and cancer. *Oncogene.* **27:** 6398–6406.
8. Mérino, D., and P. Bouillet. 2009. The bcl-2 family in autoimmune and degenerative disorders. *Apoptosis.* **14:** 570–583.
9. Takeuchi, O., J. Fisher, H. Suh, H. Harada, B. A. Malynn, and S. J. Korsmeyer. 2005. Essential role of bax,bak in b cell homeostasis and prevention of autoimmune disease. *Proc. Natl. Acad. Sci. USA.* **102:** 11272–11277.
10. Reed, J. C. 2006. Proapoptotic multidomain bcl-2//bax-family proteins: Mechanisms, physiological roles, and therapeutic opportunities. *Cell Death Differ.* **13:** 1378–1386.
11. Lindsten, T., A. J. Ross, A. King, W-X. Zong, J. C. Rathmell, H. A. Shiels, E. Ulrich, K. G. Waymire, P. Mahar, K. Frauwirth, et al. 2000. The combined functions of proapoptotic bcl-2 family members bak and bax are essential for normal development of multiple tissues. *Mol. Cell.* **6:** 1389–1399.
12. Zong, W-X., T. Lindsten, A. J. Ross, G. R. MacGregor, and C. B. Thompson. 2001. Bh3-only proteins that bind pro-survival bcl-2 family members fail to induce apoptosis in the absence of bax and bak. *Genes Dev.* **15:** 1481–1486.
13. Van Brocklyn, J. R., and J. B. Williams. 2012. The control of the balance between ceramide and sphingosine-1-phosphate by sphingosine kinase: Oxidative stress and the seesaw of cell survival and death. *Comp. Biochem. Physiol. B Biochem. Mol. Biol.* **163:** 26–36.
14. Crimi, M., and M. D. Esposti. 2011. Apoptosis-induced changes in mitochondrial lipids. *Biochim. Biophys. Acta.* **1813:** 551–557.
15. Pettus, B. J., C. E. Chalfant, and Y. A. Hannun. 2002. Ceramide in apoptosis: An overview and current perspectives. *Biochim. Biophys. Acta.* **1585:** 114–125.
16. McMillin, J. B., and W. Dowhan. 2002. Cardiolipin and apoptosis. *Biochim. Biophys. Acta.* **1585:** 97–107.
17. Zhang, T., and A. Saghatelian. 2013. Emerging roles of lipids in bcl-2 family-regulated apoptosis. *Biochim. Biophys. Acta.* **1831:** 1542–1554.
18. Kagan, V. E., V. A. Tyurin, J. Jiang, Y. Y. Tyurina, V. B. Ritov, A. A. Amoscato, A. N. Osipov, N. A. Belikova, A. A. Kapralov, V. Kini, et al. 2005. Cytochrome c acts as a cardiolipin oxygenase required for release of proapoptotic factors. *Nat. Chem. Biol.* **1:** 223–232.
19. Kagan, V. E., H. A. Bayır, N. A. Belikova, O. Kapralov, Y. Y. Tyurina, V. A. Tyurin, J. Jiang, D. A. Stoyanovsky, P. Wipf, P. M. Kochanek, et al. 2009. Cytochrome c/cardiolipin relations in mitochondria: A kiss of death. *Free Radic. Biol. Med.* **46:** 1439–1453.
20. Chipuk, J. E., G. P. McStay, A. Bharti, T. Kuwana, C. J. Clarke, L. J. Siskind, L. M. Obeid, and D. R. Green. 2012. Sphingolipid metabolism cooperates with bak and bax to promote the mitochondrial pathway of apoptosis. *Cell.* **148:** 988–1000.
21. Beverly, L. J., L. A. Howell, M. Hernandez-Corbacho, L. Casson, J. E. Chipuk, and L. J. Siskind. 2013. Bak activation is necessary and sufficient to drive ceramide synthase-dependent ceramide accumulation following inhibition of bcl2-like proteins. *Biochem. J.* **452:** 111–119.
22. Siskind, L. J., T. D. Mullen, K. Romero Rosales, C. J. Clarke, M. J. Hernandez-Corbacho, A. L. Edinger, and L. M. Obeid. 2010. The bcl-2 protein bak is required for long-chain ceramide generation during apoptosis. *J. Biol. Chem.* **285:** 11818–11826.
23. Ganesan, V., M. Perera, D. Colombini, D. Datskovskiy, K. Chadha, and M. Colombini. 2010. Ceramide and activated bax act synergistically to permeabilize the mitochondrial outer membrane. *Apoptosis.* **15:** 553–562.
24. Frezza, C., S. Cipolat, and L. Scorrano. 2007. Organelle isolation: Functional mitochondria from mouse liver, muscle and cultured filroblasts. *Nat. Protoc.* **2:** 287–295.

25. Bligh, E. G., and W. J. Dyer. 1959. A rapid method of total lipid extraction and purification. *Can. J. Biochem. Physiol.* **37:** 911–917.
26. Saghatelian, A., M. K. McKinney, M. Bandell, A. Patapoutian, and B. F. Cravatt. 2006. A faah-regulated class of n-acyl taurines that activates trp ion channels. *Biochemistry.* **45:** 9007–9015.
27. trapper (MassHunter converter). Sourceforge Sashimi Project file release. Accessed March 3, 2010, at http://sourceforge.net/projects/sashimi/files.
28. Smith, C. A., E. J. Want, G. O'Maille, R. Abagyan, and G. Siuzdak. 2006. Xcms: Processing mass spectrometry data for metabolite profiling using nonlinear peak alignment, matching, and identification. *Anal. Chem.* **78:** 779–787.
29. LMSD: LIPID MAPS structure database. Sud, M., E. Fahy, D. Cotter, A. Brown, E. Dennis, C. Glass, R. Murphy, C. Raetz, D. Russell, and S. Subramaniam. 2006. *Nucleic Acids Res.* **35:** D527–32. Accessed February 20, 2015, at. http://www.lipidmaps.org/data/structure/index.html.
30. Scripps Center for Metabolics. METLIN. Accessed February 20, 2015, at http://metlin.scripps.edu.
31. Kumar, G., S. Kaur, and V. Singh. 2011. Efficient synthesis of a styryl analogue of (2s,3r,4e)-n2-octadecanoyl-4-tetradecasphingenine via cross-metathesis reaction. *Helv. Chim. Acta.* **94:** 650–655.
32. Ojima, I., and E. S. Vidal. 1998. Rhodium-catalyzed cyclohydrocarbonylation: Application to the synthesis of (+)-prosopinine and (−)-deoxoprosophylline. *J. Org. Chem.* **63:** 7999–8003.
33. The AOCS Lipid Library. Accessed February 20, 2015, at http://lipidlibrary.aocs.org.
34. Futerman, A. H., and H. Riezman. 2005. The ins and outs of sphingolipid synthesis. *Trends Cell Biol.* **15:** 312–318.
35. Hornemann, T., A. Penno, M. F. Rütti, D. Ernst, F. Kivrak-Pfiffner, L. Rohrer, and A. von Eckardstein. 2009. The sptlc3 subunit of serine palmitoyltransferase generates short chain sphingoid bases. *J. Biol. Chem.* **284:** 26322–26330.
36. Valsecchi, M., L. Mauri, R. Casellato, S. Prioni, N. Loberto, A. Prinetti, V. Chigorno, and S. Sonnino. 2007. Ceramide and sphingomyelin species of fibroblasts and neurons in culture. *J. Lipid Res.* **48:** 417–424.
37. Emrani, J. 2005. Lipid Analysis by HPLC. *In* Encyclopedia of Chromatography, Volume 2. J. Cazes, editor. Taylor and Francis Group, Boca Raton, FL. 960–964.
38. Saghatelian, A., S. A. Trauger, E. J. Want, E. G. Hawkins, G. Siuzdak, and B. F. Cravatt. 2004. Assignment of endogenous substrates to enzymes by global metabolite profiling. *Biochemistry.* **43:** 14332–14339.
39. Yoo, H. H., J. Son, and D-H. Kim. 2006. Liquid chromatography–tandem mass spectrometric determination of ceramides and related lipid species in cellular extracts. *J. Chromatogr. B Analyt. Technol. Biomed. Life Sci.* **843:** 327–333.
40. Colsch, B., C. Afonso, I. Popa, J. Portoukalian, F. Fournier, J-C. Tabet, and N. Baumann. 2004. Characterization of the ceramide moieties of sphingoglycolipids from mouse brain by esi-ms/ms: Identification of ceramides containing sphingadienine. *J. Lipid Res.* **45:** 281–286.
41. Lee, M. H., G. H. Lee, and J. S. Yoo. 2003. Analysis of ceramides in cosmetics by reversed-phase liquid chromatography/electrospray ionization mass spectrometry with collision-induced dissociation. *Rapid Commun. Mass Spectrom.* **17:** 64–75.
42. Kelley, D. S., G. L. Bartolini, J. W. Newman, M. Vemuri, and B. E. Mackey. 2006. Fatty acid composition of liver, adipose tissue, spleen, and heart of mice fed diets containing t10, c12-, and c9, t11-conjugated linoleic acid. *Prostaglandins Leukot. Essent. Fatty Acids* **74:** 331–338.
43. Polito, A. J., T. Akita, and C. C. Sweeley. 1968. Gas chromatography and mass spectrometry of sphingolipid bases: Characterization of sphinga-4,14-dienine from plasma sphingomyelin. *Biochemistry.* **7:** 2609–2614.
44. Renkonen, O., and E. L. Hirvisalo. 1969. Structure of plasma sphingadienine. *J. Lipid Res.* **10:** 687–693.
45. Russo, S. B., R. Tidhar, A. H. Futerman, and L. A. Cowart. 2013. Myristate-derived d16:0 sphingolipids constitute a cardiac sphingolipid pool with distinct synthetic routes and functional properties. *J. Biol. Chem.* **288:** 13397–13409.
46. Danial, N. N., C. F. Gramm, L. Scorrano, C-Y. Zhang, S. Krauss, A. M. Ranger, S. Robert Datta, M. E. Greenberg, L. J. Licklider, B. B. Lowell, et al. 2003. Bad and glucokinase reside in a mitochondrial complex that integrates glycolysis and apoptosis. *Nature.* **424:** 952–956.
47. Paumen, M. B., Y. Ishida, H. Han, M. Muramatsu, Y. Eguchi, Y. Tsujimoto, and T. Honjo. 1997. Direct interaction of the mitochondrial membrane protein carnitine palmitoyltransferase i with bcl-2. *Biochem. Biophys. Res. Commun.* **231:** 523–525.
48. Giordano, A., M. Calvani, O. Petillo, P. Grippo, F. Tuccillo, M. A. B. Melone, P. Bonelli, A. Calarco, and G. Peluso. 2005. Tbid induces alterations of mitochondrial fatty acid oxidation flux by malonyl-coa-independent inhibition of carnitine palmitoyltransferase-1. *Cell Death Differ.* **12:** 603–613.
49. Pinton, P., and R. Rizzuto. 2006. Bcl-2 and Ca2+ homeostasis in the endoplasmic reticulum. *Cell Death Differ.* **13:** 1409–1418.
50. Danial, N. N., L. D. Walensky, C-Y. Zhang, C. S. Choi, J. K. Fisher, A. J. A. Molina, S. R. Datta, K. L. Pitter, G. H. Bird, J. D. Wikstrom, et al. 2008. Dual role of proapoptotic bad in insulin secretion and beta cell survival. *Nat. Med.* **14:** 144–153.
51. Karbowski, M., K. L. Norris, M. M. Cleland, S-Y. Jeong, and R. J. Youle. 2006. Role of bax and bak in mitochondrial morphogenesis. *Nature.* **443:** 658–662.
52. Lee, H., J. A. Rotolo, J. Mesicek, T. Penate-Medina, A. Rimner, W-C. Liao, X. Yin, G. Ragupathi, D. Ehleiter, E. Gulbins, et al. 2011. Mitochondrial ceramide-rich macrodomains functionalize bax upon irradiation. *PLoS One.* **6:** e19783.
53. Stiban, J., D. Fistere, and M. Colombini. 2006. Dihydroceramide hinders ceramide channel formation: Implications on apoptosis. *Apoptosis.* **11:** 773–780.
54. Hartmann, D., J. Lucks, S. Fuchs, S. Schiffmann, Y. Schreiber, N. Ferreirós, J. Merkens, R. Marschalek, G. Geisslinger, and S. Grösch. 2012. Long chain ceramides and very long chain ceramides have opposite effects on human breast and colon cancer cell growth. *Int. J. Biochem. Cell Biol.* **44:** 620–628.
55. Fyrst, H., X. Zhang, D. R. Herr, H. S. Byun, R. Bittman, V. H. Phan, G. L. Harris, and J. D. Saba. 2008. Identification and characterization by electrospray mass spectrometry of endogenous drosophila sphingadienes. *J. Lipid Res.* **49:** 597–606.
56. Lynch, D. V., and T. M. Dunn. 2004. An introduction to plant sphingolipids and a review of recent advances in understanding their metabolism and function. *New Phytol.* **161:** 677–702.
57. Merrill, A. H., Jr. 1983. Characterization of serine palmitoyltransferase activity in chinese hamster ovary cells. *Biochim. Biophys. Acta.* **754:** 284–291.
58. Williams, R. D., E. Wang, and A. H. Merrill, Jr. 1984. Enzymology of long-chain base synthesis by liver: Characterization of serine palmitoyltransferase in rat liver microsomes. *Arch. Biochem. Biophys.* **228:** 282–291.
59. Farwanah, H., B. Pierstorff, C. E. H. Schmelzer, K. Raith, R. H. H. Neubert, T. Kolter, and K. Sandhoff. 2007. Separation and mass spectrometric characterization of covalently bound skin ceramides using lc/apci-ms and nano-esi-ms/ms. *J. Chromatogr. B Analyt. Technol. Biomed. Life Sci.* **852:** 562–570.
60. Han, X. 2002. Characterization and direct quantitation of ceramide molecular species from lipid extracts of biological samples by electrospray ionization tandem mass spectrometry. *Anal. Biochem.* **302:** 199–212.
61. Hsu, F-F., J. Turk, M. Stewart, and D. Downing. 2002. Structural studies on ceramides as lithiated adducts by low energy collisional-activated dissociation tandem mass spectrometry with electrospray ionization. *J. Am. Soc. Mass Spectrom.* **13:** 680–695.
62. Hsu, F. F., and J. Turk. 2002. Characterization of ceramides by low energy collisional-activated dissociation tandem mass spectrometry with negative-ion electrospray ionization. *J. Am. Soc. Mass Spectrom.* **13:** 558–570.
63. Ann, Q., and J. Adams. 1993. Structure-specific collision-induced fragmentations of ceramides cationized with alkali-metal ions. *Anal. Chem.* **65:** 7–13.